# The crustal structure beneath the northwest of the Zagros (Kermanshah Region) from teleseismic receiver functions

Afsari, N.[1][*], Sodoudi, F.[2], Gheitanchi, M. R.[3], Kaviani, A.[4] and Taghizadeh-Farahmand, F.[5]

[1] Ph. D. Student of Seismology, Islamshahr Branch, Islamic Azad University, Tehran, Iran
[2] Helmholtz Center Potsdam, GFZ Research Center for Geosciences, Telegrafenberg 14473 Potsdam, Germany
[3] Professor, Earth Physics Department, Institute of Geophysics, University of Tehran, Iran
[4] Assistant Professor, Geophysic Department, Institute for Advanced Studies in Basic Science, Zanjan, Iran.
[5] Assistant Professor, Department of Physics, Qom Branch, Islamic Azad University, Qom, Iran

## Abstract

In this study, we used teleseismic data which was recorded by 5 stations (DHR, GHG, KOM, LIN and VIS) of the Kermanshah Seismic Network from 2003 to 2007 with $M_b \geq 5.5$ and epicentral distances from 30° to 95°. The crustal structure beneath these stations was determined by the modeling of the P receiver functions. The main phases, which were observed in our final P receiver functions, are Moho conversions, their multiples in the crust, and conversions at the base of the sediments. We obtained a 2-layer model for the crust of the Kermanshah Region. The crust beneath this region is approximately 42 km thick and consists of a 9 to 18 km thick sedimentary layer overlying a 24 to 35 km thick layer. The average shear wave velocity was estimated to be 3.69 $kms^{-1}$ in the crust and reaches to 4.80 $kms^{-1}$ under Moho and those obtained from other geophysical studies.

## ساختار پوسته‌ای زیر شمال غرب زاگرس (منطقه کرمانشاه) با استفاده از توابع گیرنده دورلرز

نرگس افسری¹، فروغ صدودی²، محمدرضا قیطانچی³، ایوب کاویانی⁴ و فتانه تقی‌زاده فرهمند⁵

¹ دانشجوی دکتری زلزله‌شناسی، دانشگاه آزاد اسلامی واحد اسلامشهر، تهران، ایران
² پژوهشگر، مؤسسه تحقیقاتی علوم زمین هلمهولتز، پتسدام، آلمان
³ استاد، گروه فیزیک زمین، مؤسسة ژئوفیزیک دانشگاه تهران، ایران
⁴ استادیار، دانشکده ژئوفیزیک، مرکز تحصیلات تکمیلی علوم پایه، زنجان، ایران
⁵ استادیار، گروه فیزیک دانشکده علوم دانشگاه آزاد اسلامی واحد قم، ایران

### چکیده

همان‌طور که می‌دانیم یکی از هدف‌های مهم تحقیقات ژئوفیزیکی، به‌دست آوردن مدل سرعتی مناسب برای پوسته است. با استفاده از وارون‌کردن توابع گیرنده می‌توان به برآورد درستی از ساختار سرعتی موج برشی زیر یک ایستگاه لرزه‌ای دست یافت. در این تحقیق برای مدل‌سازی از روشی که کیند و همکاران (۱۹۹۵) بیان کرده‌اند، استفاده کرده‌ایم. در ابتدا فرض می‌کنیم که پوسته زمین از لایه‌های تخت همگن که روی یک نیم‌فضای همگن قرارگرفته‌اند تشکیل شده است. سپس لرزه‌نگاشت‌های نظری موج تخت برای مدل اولیه محاسبه می‌شود. نگاشت‌های نظری با همان روش نگاشت‌های مشاهده‌ای چرخانده و سپس واهم‌آمیخت شده‌اند.

---

[*]Corresponding author:   Tel: 021-88263939   Fax: 021-88630548   E-mail: ng_afsari@yahoo.com

برای مدل‌سازی ابتدا همه مولفه‌های L و Q توابع گیرنده در هرایستگاه را بعد از فیلترکردن بر انبارش می‌کنیم. عمل وارون‌سازی در پنجره زمانی به طول ۳۵ ثانیه (۳۰ ثانیه بعد از شروع موج P و ۵ ثانیه قبل ازآن) که همه تبدیلات پوسته‌ای و بازتاب‌های مربوط به آنها را در برداشته باشد، صورت گرفته است. بهینه پارامترهای مدل با روش سعی و خطا و کمینه‌کردن اختلاف جذر میانگین مربعی بین توابع گیرنده مشاهده‌ای و نظری و همچنین مدل‌های اولیه و نهایی به‌دست می‌آیند. با توجه به وابسته بودن جواب روش وارون‌سازی به مدل اولیه انتخاب شده، برای به‌دست آوردن بهترین مدل سرعتی موج برشی و محاسبه دقیق‌تر عمق موهو از مدل‌های اولیه متفاوتی برای هر ایستگاه استفاده شد. مدل‌های اولیه براساس اطلاعات موجود روی توابع گیرنده و نتایج به‌دست آمده از تحقیقات هاتزفلد و همکاران (۲۰۰۳) و پل و همکاران (۲۰۰۶) انتخاب شد و با روش سعی و خطا، تفاوت توابع گیرنده مشاهده‌ای و محاسبه‌ای را به حداقل رساندیم. در ابتدا از دهها مدل اولیه با در نظرگرفتن لایه‌هایی به ضخامت‌های متفاوت و با ضخامت کل ۶۰ کیلومتر (با توجه به محتوی بسامدی و فیلتر به کار رفته، حداکثر ۳۰ لایه و با ضخامت ۲ کیلومتر) در بازه سرعتی ۵ تا ۷کیلومتر بر ثانیه برای موج P، استفاده شد. از میان همه مدل های اولیه در مرحله اول، مدل‌هایی که مدل‌های نهایی به‌دست آمده از آنها همگرایی قابل قبولی داشتند و خطای جذر میانگین مربعی آنها کمتر از ۰٫۰۲۵s بود، نگه داشتیم. برای به‌دست آوردن بهینه مدل نهایی در مرحله دوم متوسط مدل‌های نهایی به‌دست آمده در مرحله اول که همگرایی خوبی داشتند، مبنا قرار داده شد و با توجه به توابع گیرنده محاسبه شده برای منطقه که دارای دو فاز تبدیلی تا موهومی باشند، مدل‌های متفاوت درحکم ورودی مرحله دوم انتخاب شدند. در این مرحله ضخامت کل ۶۰ کیلومتری در هر مدل ورودی به دو لایه با ضخامت‌های متفاوت در نظر گرفته شد. مدل‌های خروجی که همگرایی خوبی با یکدیگر داشتند و خطای میانگین مربعی آنها کمتر از ۰٫۰۵s بود، به‌منزلهٔ مدل‌های نهایی قابل قبول برای مدل سرعتی موج برشی منطقه انتخاب شدند و متوسط آنها را درحکم بهینه مدل برای پوسته زیر هر ایستگاه در نظرگرفتیم. با توجه به توابع گیرنده محاسبه شده برای هر ایستگاه و مدل‌های به دست آمده، مدل نهایی حاصل برای منطقه کرمانشاه، یک مدل دو لایه است. متوسط ضخامت پوسته زیر این منطقه تقریبا ۴۲ کیلومتر است که تشکیل شده از لایه‌ای رسوبی است که ضخامت آن از ۹ تا ۱۸ کیلومتر تغییر می‌کند و روی لایه‌ای به‌ضخامت ۲۴ تا ۳۵ کیلومتر قرار گرفته است و با نتایج به دست آمده از دیگر تحقیقات ژئوفیزیکی همخوانی دارد. همچنین متوسط سرعت موج برشی در پوسته منطقه $3{,}69$ kms$^{-1}$ به‌دست آمد که در زیر ناپیوستگی موهو به $4{,}8$ kms$^{-1}$ می‌رسد.

واژه‌های کلیدی: وارون‌سازی– عمق موهو– مدل‌سازی داده‌های دورلرز– تابع گیرنده P — ساختار پوسته

## 1 INTRODUCTION

Moho discontinuity which separates the Earth's crust from the underlying mantle represents a major change in seismic velocities and chemical compositions. The depth of Moho and the average velocity of crust are important parameters to characterize the overall structure of the crust and can often be related to the geology and tectonic evolution of the region. The usual methods to explore the crustal and lithospheric structure by seismic methods are reflection and refraction methods which have the highest resolution because of the relatively high frequency of the seismic waves used. Teleseismic body waves have been intensively used to investigate crust and upper mantle structure. The receiver function method has been applied to delineate crustal thickness and occasionally other first-order details of the continental crust (Phinney,

1964; Burdick and Laneston, 1977; Langston, 1977 and 1979; Vinnik and Kosarev, 1981). With the advent of digital seismic stations higher resolution crustal models could be determined beneath isolated stations (Owens et al., 1984 and 1987). The only available profiles of crustal thickness variations have been computed from Bouguer anomaly modeling by Dehghani and Makris (1984) for the whole of Iran, and Snyder and Barazangi (1986) for the Zagros. Hatzfeld et al. (2003) estimated a crustal thickness of 46 ± 2 km from receiver function (RFs) computed at a single station close to the town of Ghir in the central Zagros.

Pual et al. (2006) using the migrated section computed from radial RFs, obtained from the coast of the Persian Gulf to 25 km southwest of the Main Zagros Thrust (MZT), the Moho is almost horizontal with slight

depth variations around 45 km. Afsari et al., (2008) applying the Zhu and Kanamori (2000) method northwest of the Zagros (Kermanshah Region) determined that the Moho depth is 40 km on average. In this study, to improve our knowledge about the crustal structure beneath the Kermanshah Region as well as to map the Moho discontinuity beneath the northwest of the Zagros, which belongs to the most active areas in Iran, we used the receiver function inversion method (Kind et al., 1995). According to IASP91, this procedure results in 2 km error in the Moho depth determination.

## 2 TECTONIC SETTING

Iran is located along the Alpine-Himalayan orogenic belt. The Zagros mountain range, running from eastern Turkey to the Gulf of Oman, has long been thought of as a classic fold and thrust system. The active Zagros fold-thrust belt lies on the northeastern margin of the Arabian plate, on Precambrian (Pan African) basement. The present velocity of Arabia with respect to Eurasia is approximately $22 \pm 2$ mmyr$^{-1}$ in the direction N8° $\pm$ 5°E (Vernant el al., 2004). This convergence is accommodated by crustal shortening by fold-and-thrust deformation and thickening in the Zagros (Kaviani et al., 2007). The MZRF indicates a fundamental change in sedimentary history, palegeography, structure, morphology and seismicity. It marks the suture between the two colliding plates of the central Iranian active continental margin (to the northeast) and the Afro-Arabian passive continental margin, the Zagros fold-thrust belt to the southwest (Berberian, 1995). The MRF (Tchalenco and Braud, 1974) is a major seismically active right-lateral strike-slip fault with a NW-SE trend which more or less follows the trace of the MZRF (Berberian, 1995). The MRF is morphologically and structurally distinct along its entire length, and the component of right-lateral strike-slip motion between Arabia and central Iran is taking place preferentially along different segments of the MRF in western Iran

(Jackson, 1992). The HZF (the southern boundary of the thrust zone of Berberian and Tchalenko, 1976a and b) separates the thrust belt of the High Zagros, (in the southwest). The High Zagros is characterized by extensively deformed overthrust anticlines mainly composed of autochthonous Jurassic-Cretaceous outcrops with Paleozoic cores along the reverse faults, allochthonous Jurassic-Cretaceous limestone of the Bisutun seamount, obductde Upper Cretaceous radiolarite-ophiolite nappes, Upper Cretaceous to Eocene-Oligocene fiych and longitudinal reverse faults. Seismicity in the Zagros belt is restricted to the region between the Main Zagros Thrust and the Persian Gulf. Most of the larger earthquakes occur on high-angle reverse planes striking parallel to the trend of the fold axes (Jackson, 1980; Jackson and MacKenzie, 1984). The region referred to in this study as northwest Zagros is enclosed between 45°-49° east longitudes and 33°-36° north latitudes (figure 1).

## 3 THE METHOD OF ANALYSIS

Receiver functions are frequently modeled with 1-D crustal and uppermost mantle shear wave velocity changes. The method, which was used in this study, is the P receiver function. This method results in detecting the P-to-S converted waves at discontinuities underneath a seismic station. The inversion analysis consists of two steps. The data are first processed in order to produce stable observations (see also Afsari et al., 2008). The second step consists of the inversion of the observations using complete theoretical plane-wave seismograms. The essential points in processing the observed data are as follows:

1) Rotation of Z, N, and E components into the ray coordinate system L, Q, and T. The L component contains mainly P energy and points in the direction of P wave incident to the surface. The Q component contains mainly SV energy and is in the ray plane and perpendicular to L. The T component is perpendicular to both L and Q, and forming the third axis of the right hand LQT system. Large energy on T component reflects

anisotropic or laterally inhomogeneous structure and/ or dipping interfaces beneath the receiver (Langston, 1977). The eigenvalues of the covariance matrix are used for the calculation of the rotation angles (incidence angle and back-azimuth) over a time window spanning the first few seconds following the P arrival (e.g. Kind et al., 1995). The Q and T components contain information on the structure beneath a seismic station .The amplitude of the converted Ps phase depends on the S wave velocity distribution underneath the station.

2) Deconvolution of the Q and T component with the P signal on the L component). This procedure removes the effects of the source region and the propagation path. Deconvolution can be performed both in the frequency and in the time domains. The deconvolution method described in Kind et al. (1995) is used, which generates the inverse filter in the time domain by minimizing the least-square different between the observed seismogram and the desired delta – like spike function of normalized amplitude. The P waveform on the L component is used to generate the deconvolution filter. After deconvolution, all components are normalized to the maximum of L.

3) Summation of many events from a large distance and azimuth range. The summation of rotated and deconvolved records from earthquakes with epicenters in a broad azimuth and distance range is used to improve the signal-to-noise rate and therefore the stability and reliability of the observations. This kind of summation results in a flat and average crustal model.

## 3.1 INVERSION METHOD

The method, which was used for the inversion of the P receiver functions, is described by Kind et al. (1995). We consider the theoretical L and Q component ($Q_{syn}$) of the teleseismic P wave computed on the Earth's surface, and assume that the Earth's crust can be modeled by a stack of plane homogeneous layers over a homogeneous half-space. The P wave front is considered to

be a plane wave. The theoretical seismograms used in the inversion method have been computed for the starting model using the method of Haskell (1962) for an angle of incidence averaged over all epicentral distances of the recorded receiver functions. The observed Q component ($Q_{obs}$) is the sum of all Q component used. The theoretical traces are rotated and deconvolved in the same manner as the observed traces. The model of velocity can be tested by comparing $Q_{syn}$ with $Q_{obs}$. The optimal parameters of the model are found by iteratively minimizing the root mean square difference of the observed and theoretical traces and the starting and final models (Kind et al., 1995). P receiver functions at station KOM were stacked to get the average velocity structure under the station. The stacked Q and L components for KOM station are represented in figure 2. One example of the inversion method is shown in figure 3. The thin line in the model on the left represents the starting model and the heavy line represents the final model. Adjacent to the model, the dashed line represents the data, the thin line belongs to the starting model and the heavy line belongs to the final model. The top trace on the right is the deconvolved P signal of the L component with its amplitude normalized to one. The amplitude scale of the Q component is marked, and is different from the amplitude scale of the P signal. The starting model is a shear velocity model. The P velocity was fixed with a Poisson's ratio of 0.25 and the density was fixed by Birch's law (Birch, 1961). The Fit between the theoretical seismograms of the final model and the data seems reasonable. The applied inversion method is not unique, since it tries to find, by definition, models close to the starting model and the final model depends on the choice of a physically reasonable starting model (Ammon, 1990). We did the inversion by choosing the simplest starting model and then adding a priori information.

## 4 DATA AND RESULTS

The data used in this study are teleseismic

data (30°<Δ<95°) with $m_b \geq 5.5$ which were recorded at six short-period three component stations (BZA, DHR, GHG, KOM, LIN, VIS) between 2003 and 2007. These stations are equipped with SS-1 seismometers with frequency response of 1 HZ. Table 1 contains the list of station names and coordinates. figure 4 shows epicenter distribution of earthquakes used to determine P receiver function s.
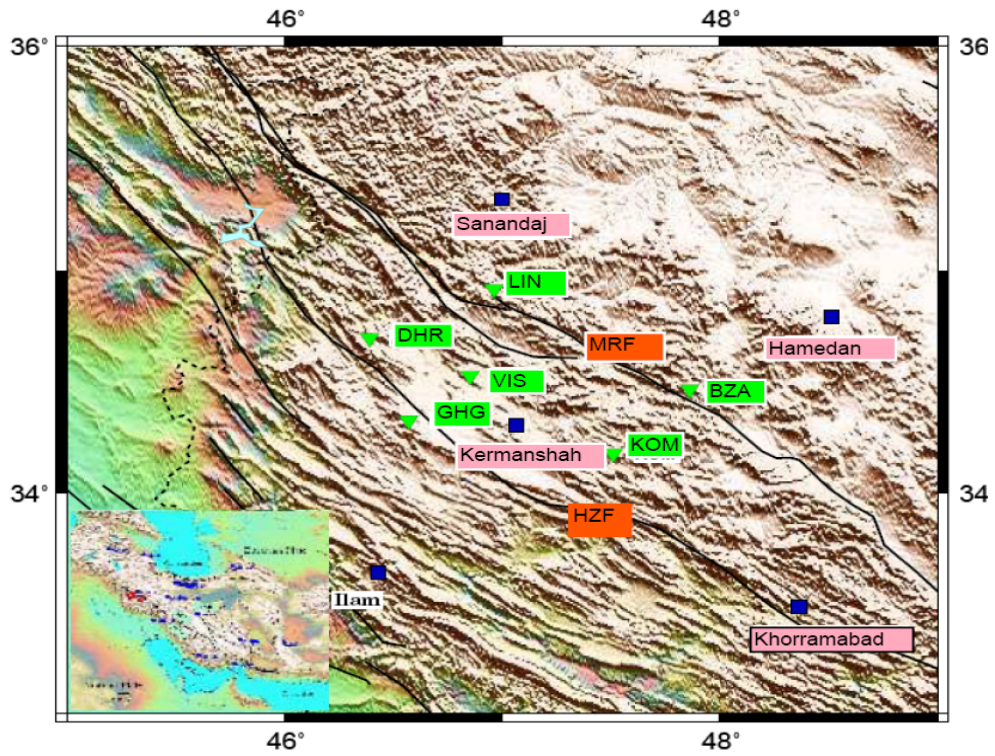


**Figure 1.** Location map of the seismological Network. stations used in this the study are plotted in with green reverse triangles. MRF and HZF, represent Main Recent Fault and High Zagros fault, respectively.
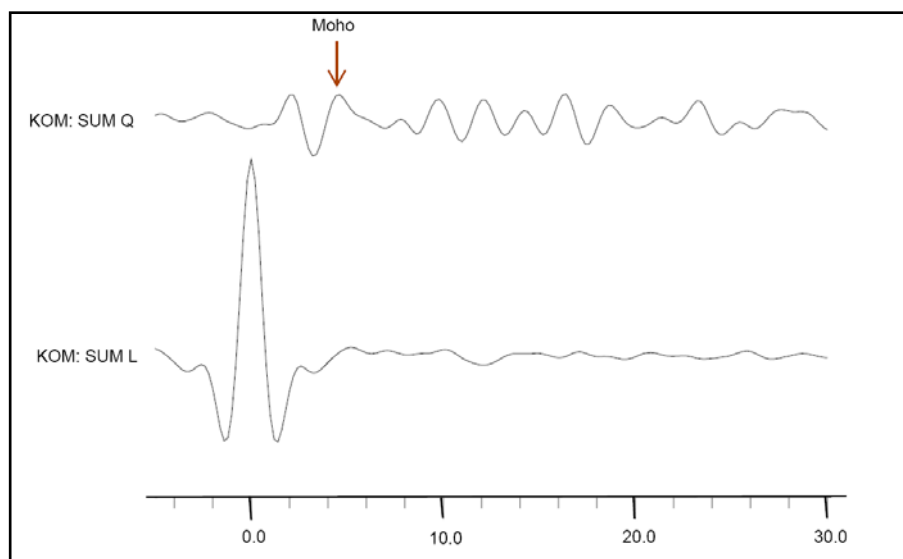


**Figure 2.** The stacked Q and L components for KOM station.
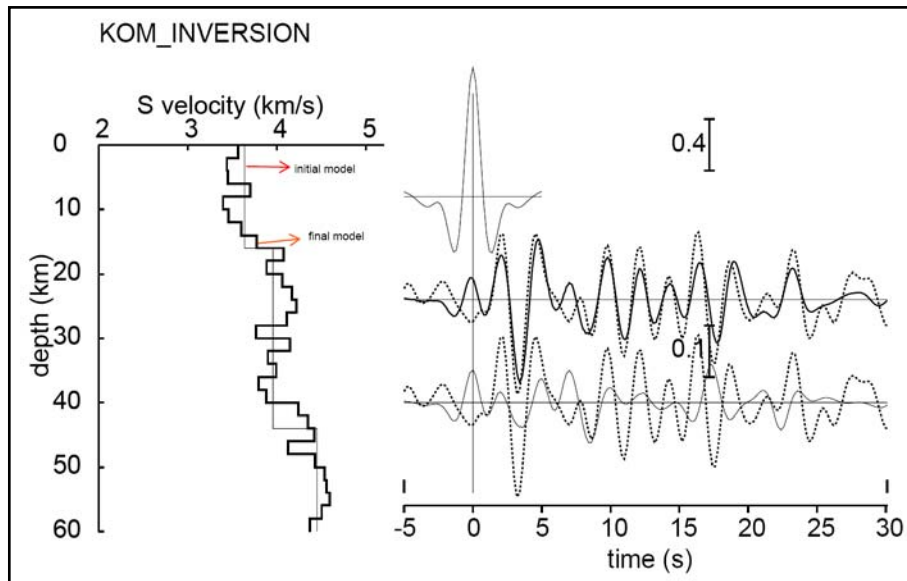
**Figure 3.** Receiver function inversion of the permanent station KOM. Starting and final models are shown by thin and thick lines in the left, respectively. The dashed line on the right is the observed receiver function (Q component), solid lines are synthetic receiver functions for the starting model ( thin line at the bottom) and for the final model (thick line of the middle traces). The top trace on the right is the input P signal (L component), which has the normalized amplitude of 1. The amplitude scale of the Q component is shown.

**Table 1.** Lists seismic stations used in this study.

| Station name | Station code | Latitude (Deg.) | Longitude (Deg.) | Elevation   (m) |
|---|---|---|---|---|
| Dehrash | DHR | 34.6997 | 46.3860 | 1434 |
| Ghaleghazi | GHG | 34.3294 | 46.5686 | 2090 |
| Komasi | KOM | 34.1764 | 47.5144 | 1502 |
| Lien | LIN | 34.9186 | 46.9624 | 2195 |
| Veis | VIS | 34.5253 | 46.8527 | 1135 |

**Table 2.** List of the teleseismic earthquakes used in this study.

| Year | Month | Day | Time | Lat. (Deg.) | Lon. (Deg.) | Depth(km) | Mb | Epicentral Distance (km) |
|---|---|---|---|---|---|---|---|---|
| 2004 | 1 | 11 | 43247.79 | -36.7 | 53.35 | 5 | 6.1 | 7916 |
| 2004 | 1 | 16 | 180755.66 | 7.64 | -37.7 | 10 | 5.9 | 9051 |
| 2004 | 1 | 19 | 72252.91 | 84.47 | 105.21 | 10 | 5.6 | 5890 |
| 2004 | 1 | 24 | 130145.7 | 52.12 | -30.18 | 10 | 5.9 | 6256 |
| 2004 | 1 | 28 | 221530.7 | -3.12 | 127.4 | 17 | 6.7 | 9306 |
| 2004 | 1 | 29 | 94842.76 | 6.29 | 126.94 | 209 | 5.7 | 8678 |
| 2004 | 1 | 30 | 175144.82 | 44.73 | 150.06 | 30 | 5.5 | 8313 |
| 2004 | 2 | 7 | 24235.21 | -4 | 135.02 | 10 | 7.5 | 10058 |
| 2004 | 2 | 10 | 203351.26 | 59.37 | -152.03 | 65 | 5.6 | 9474 |

| 2004 | 2 | 24 | 22746.23 | 35.14 | -4 | 0 | 6.4 | 4623 |
|------|----|----|-----------|--------|---------|-----|-----|-------|
| 2004 | 2 | 28 | 52354.42 | -18.73 | -12.56 | 11 | 5.7 | 8611 |
| 2004 | 3 | 24 | 15349.43 | 45.38 | 118.26 | 18 | 5.6 | 6006 |
| 2004 | 3 | 26 | 152006.62 | 41.86 | 144.21 | 22 | 5.8 | 8079 |
| 2004 | 4 | 3 | 230200.87 | 36.43 | 141.01 | 31 | 5.7 | 8148 |
| 2004 | 4 | 9 | 15550.71 | -1.55 | 100.54 | 65 | 5.5 | 6831 |
| 2004 | 4 | 14 | 230739.94 | 71.07 | -7.75 | 12 | 5.8 | 5116 |
| 2004 | 4 | 14 | 15409.22 | 55.23 | 162.66 | 51 | 6 | 8351 |
| 2004 | 4 | 16 | 215705.41 | -5.21 | 102.72 | 44 | 5.6 | 7280 |
| 2004 | 4 | 17 | 190055.18 | -6.39 | 129.98 | 157 | 5.7 | 9747 |
| 2004 | 4 | 23 | 15030.22 | -9.36 | 122.84 | 65 | 6.5 | 9297 |
| 2004 | 5 | 6 | 134312.89 | 42.53 | 145.02 | 28 | 5.6 | 8099 |
| 2004 | 5 | 8 | 80254.22 | 21.95 | 121.6 | 26 | 5.7 | 7283 |
| 2004 | 5 | 19 | 70411.71 | 22.66 | 121.5 | 20 | 5.8 | 7236 |
| 2004 | 5 | 29 | 205609.6 | 34.25 | 141.41 | 16 | 5.6 | 8303 |
| 2004 | 6 | 10 | 151957.75 | 55.68 | 160 | 188 | 6.1 | 8188 |
| 2004 | 6 | 28 | 94947 | 54.8 | -134.25 | 20 | 6.8 | 10132 |
| 2004 | 6 | 30 | 233725.45 | 0.8 | 124.73 | 90 | 6.3 | 8816 |
| 2004 | 7 | 8 | 103049.16 | 47.2 | 151.3 | 128 | 6.4 | 8242 |
| 2004 | 7 | 11 | 230844.18 | 30.69 | 83.67 | 13 | 6.2 | 3438 |
| 2004 | 7 | 24 | 185458.27 | 26.49 | 128.75 | 30 | 5.5 | 7677 |
| 2004 | 7 | 28 | 35628.6 | -0.44 | 133.09 | 13 | 6.5 | 9659 |
| 2004 | 7 | 29 | 14406.91 | 12.45 | 95 | 22 | 5.9 | 5393 |
| 2004 | 8 | 2 | 23654.94 | -5.47 | 102.62 | 40 | 5.6 | 7290 |
| 2004 | 8 | 6 | 143527.03 | 12.43 | 95 | 23 | 5.7 | 5395 |
| 2004 | 8 | 10 | 61333.24 | 39.63 | 141.96 | 69 | 5.7 | 8041 |
| 2004 | 8 | 30 | 122321.6 | 49.54 | 157.28 | 11 | 5.7 | 8454 |
| 2004 | 9 | 5 | 100707.82 | 33.07 | 136.62 | 14 | 6.7 | 7987 |
| 2004 | 9 | 6 | 232935.09 | 33.21 | 137.23 | 10 | 6.4 | 8029 |
| 2004 | 9 | 8 | 145825.83 | 33.14 | 137.2 | 21 | 6.2 | 8030 |
| 2004 | 9 | 13 | 30012.85 | 44 | 151.41 | 8 | 6 | 8448 |
| 2004 | 9 | 15 | 191050.6 | 14.22 | 120.41 | 115 | 6 | 7604 |
| 2004 | 9 | 19 | 202604.1 | 52.21 | 174.03 | 25 | 5.6 | 9125 |
| 2004 | 9 | 28 | 152953.82 | -52.51 | 28.02 | 10 | 5.9 | 9791 |
| 2004 | 10 | 4 | 192034.98 | 14.55 | 146.99 | 7 | 5.9 | 9984 |
| 2004 | 10 | 8 | 143606.11 | 13.93 | 120.53 | 105 | 6.3 | 7633 |
| 2004 | 10 | 15 | 40850.24 | 24.53 | 122.69 | 94 | 6.4 | 7245 |
| 2004 | 10 | 16 | 185443.56 | 36.24 | 141.3 | 47 | 5.5 | 8182 |
| 2004 | 10 | 23 | 103645.81 | 37.22 | 138.64 | 10 | 5.7 | 7921 |
| 2004 | 10 | 24 | 210457.06 | 37.31 | 138.7 | 11 | 6 | 7922 |
| 2004 | 10 | 24 | 133115.51 | -6.57 | 130.22 | 89 | 5.5 | 9780 |
| 2004 | 10 | 27 | 14050.26 | 37.28 | 138.88 | 14 | 5.7 | 7937 |
| 2004 | 10 | 28 | 83207 | -4.91 | 103.21 | 42 | 5.6 | 7298 |
| 2004 | 10 | 29 | 192857.52 | 15.64 | 119.11 | 21 | 5.5 | 7403 |
| 2004 | 11 | 2 | 130424.36 | 38.84 | 142.77 | 23 | 5.5 | 8146 |
| 2004 | 11 | 2 | 84556.28 | 28.7 | 143.21 | 10 | 5.6 | 8776 |
| 2004 | 11 | 4 | 140311.67 | 43.62 | 146.81 | 61 | 5.8 | 8160 |
| 2004 | 11 | 8 | 155501.15 | 24.1 | 122.54 | 29 | 5.9 | 7253 |

| 2004 | 11 | 8 | 21558.84 | 37.4 | 138.86 | 10 | 5.6 | 7929 |
|---|---|---|---|---|---|---|---|---|
| 2004 | 11 | 11 | 21645.29 | 24.41 | 122.23 | 49 | 5.7 | 7209 |
| 2004 | 12 | 26 | 101931.73 | 13.46 | 92.74 | 26 | 6.1 | 5129 |
| 2004 | 12 | 26 | 73827 | 13.13 | 93.04 | 30 | 5.7 | 5176 |
| 2004 | 12 | 26 | 92001.61 | 8.88 | 92.38 | 16 | 6 | 5400 |
| 2004 | 12 | 26 | 70710.27 | 10.36 | 93.75 | 19 | 5.6 | 5419 |
| 2004 | 12 | 26 | 60228.38 | 8.27 | 94.06 | 23 | 5.7 | 5586 |
| 2004 | 12 | 27 | 144646.49 | 12.35 | 92.47 | 19 | 5.8 | 5176 |
| 2004 | 12 | 28 | 111743.87 | 4.73 | 95.21 | 36 | 5.8 | 5931 |
| 2004 | 12 | 29 | 55647.54 | 8.79 | 93.2 | 12 | 5.8 | 5477 |
| 2004 | 12 | 29 | 13941.24 | 8.38 | 93.16 | 34 | 5.5 | 5501 |
| 2004 | 12 | 29 | 15052.57 | 9.11 | 93.76 | 8 | 6 | 5503 |
| 2004 | 12 | 29 | 211259.47 | 5.23 | 94.62 | 29 | 5.7 | 5846 |
| 2004 | 12 | 30 | 175811.19 | 12.24 | 92.51 | 30 | 5.8 | 5188 |
| 2004 | 12 | 30 | 10451.82 | 4.23 | 94.22 | 16 | 5.5 | 5883 |
| 2004 | 12 | 31 | 22400.52 | 7.12 | 92.53 | 14 | 5.7 | 5535 |
| 2004 | 12 | 31 | 143846.62 | 5.11 | 94.86 | 49 | 5.6 | 5874 |
| 2005 | 1 | 1 | 62544.82 | 5.1 | 92.3 | 11 | 6 | 5660 |
| 2005 | 1 | 1 | 40310.99 | 5.47 | 94.4 | 36 | 5.8 | 5811 |
| 2005 | 1 | 4 | 91312.25 | 10.67 | 92.36 | 23 | 6 | 5277 |
| 2005 | 1 | 6 | 5629.91 | 5.32 | 94.83 | 49 | 6.1 | 5858 |
| 2005 | 1 | 9 | 221256.51 | 4.93 | 95.11 | 40 | 6 | 5909 |
| 2005 | 1 | 16 | 201752.76 | 10.93 | 140.84 | 24 | 6.3 | 9663 |
| 2005 | 1 | 17 | 105032.56 | 10.99 | 140.68 | 12 | 5.9 | 9646 |
| 2005 | 1 | 24 | 41647.44 | 7.33 | 92.48 | 30 | 6.1 | 5516 |
| 2005 | 1 | 26 | 173028.82 | 8.25 | 94.04 | 23 | 5.6 | 5586 |
| 2005 | 1 | 26 | 220042.57 | 2.7 | 94.6 | 22 | 5.6 | 6026 |
| 2005 | 2 | 9 | 184609.97 | 26.09 | 144 | 24 | 6.2 | 9000 |
| 2005 | 2 | 14 | 170652.64 | -0.13 | 98.73 | 47 | 6 | 6577 |
| 2005 | 2 | 17 | 53128.08 | 4.7 | 95.16 | 47 | 5.9 | 5929 |
| 2005 | 2 | 19 | 443.59 | -5.56 | 122.13 | 10 | 6.3 | 8986 |
| 2005 | 2 | 26 | 123740.69 | 40.73 | 142.38 | 68 | 5.8 | 8011 |
| 2005 | 3 | 2 | 104212.23 | -6.53 | 129.93 | 201 | 7 | 9751 |
| 2005 | 3 | 28 | 183044.56 | 0.92 | 97.87 | 36 | 6.1 | 6428 |
| 2005 | 4 | 9 | 151627.89 | 56.17 | -154.52 | 14 | 5.8 | 9773 |
| 2005 | 4 | 10 | 102911.28 | -1.64 | 99.61 | 19 | 6.4 | 6760 |
| 2005 | 4 | 10 | 172439.4 | -1.59 | 99.72 | 30 | 5.9 | 6766 |
| 2005 | 4 | 10 | 111419.62 | -1.71 | 99.78 | 30 | 6.2 | 6780 |
| 2005 | 4 | 10 | 222215.71 | 35.6 | 140.4 | 43 | 6.1 | 8148 |
| 2005 | 4 | 11 | 61111.82 | 2.17 | 96.76 | 24 | 5.9 | 6245 |
| 2005 | 4 | 14 | 112952.55 | -1.91 | 99.95 | 33 | 5.8 | 6809 |
| 2005 | 4 | 16 | 163803.9 | 1.81 | 97.66 | 31 | 6 | 6347 |
| 2005 | 4 | 17 | 134354.56 | 0.31 | 97.66 | 25 | 5.7 | 6456 |
| 2005 | 4 | 17 | 212350.83 | -1.63 | 99.62 | 21 | 5.8 | 6760 |
| 2005 | 5 | 9 | 13052.51 | 5.1 | 94.84 | 30 | 5.5 | 5874 |
| 2005 | 5 | 10 | 10905.1 | -6.23 | 103.14 | 17 | 5.9 | 7388 |
| 2005 | 6 | 1 | 200641.45 | 28.88 | 94.63 | 25 | 6.1 | 4505 |
| 2005 | 6 | 12 | 41713.49 | 52.79 | 143.87 | 10 | 5.6 | 7468 |

| 2005 | 6 | 14 | 171012.28 | 51.24 | 179.31 | 17 | 6.1 | 9441 |
|---|---|---|---|---|---|---|---|---|
| 2005 | 6 | 26 | 82303.87 | 1.77 | 125.82 | 91 | 6 | 8855 |
| 2005 | 7 | 4 | 113605.65 | -42.28 | 42.37 | 10 | 5.7 | 8490 |
| 2005 | 7 | 9 | 233711.14 | 33.42 | 140.82 | 55 | 5.8 | 8305 |
| 2005 | 7 | 12 | 170719.82 | -6.83 | 131.4 | 39 | 5.6 | 9904 |
| 2005 | 7 | 24 | 154206.21 | 7.92 | 92.19 | 16 | 6.6 | 5450 |
| 2005 | 7 | 29 | 203340.03 | 2.86 | 93.56 | 32 | 5.8 | 5928 |
| 2005 | 8 | 7 | 21746.04 | -47.09 | 33.62 | 10 | 5.7 | 9110 |
| 2005 | 8 | 13 | 73652.77 | 20.13 | 145.8 | 48 | 5.8 | 9524 |
| 2005 | 8 | 30 | 181045.46 | 38.48 | 143.18 | 21 | 5.8 | 8197 |
| 2005 | 9 | 10 | 165747.27 | 4.86 | 95.04 | 41 | 5.8 | 5908 |
| 2005 | 9 | 12 | 215106.69 | -7.66 | 125.5 | 30 | 5.5 | 9422 |
| 2005 | 9 | 21 | 22508.11 | 43.89 | 146.15 | 103 | 6 | 8099 |
| 2005 | 10 | 11 | 150539.7 | 4.82 | 95.1 | 30 | 6 | 5916 |
| 2005 | 10 | 15 | 100617 | 46.82 | 154.11 | 42 | 6 | 8442 |
| 2005 | 10 | 29 | 40556.04 | -45.21 | 96.9 | 8 | 6.1 | 10128 |
| 2005 | 11 | 14 | 213851.4 | 38.11 | 144.9 | 11 | 6.7 | 8347 |
| 2005 | 11 | 19 | 141013.03 | 2.16 | 96.79 | 21 | 6 | 6248 |
| 2005 | 12 | 2 | 131309.52 | 38.09 | 142.12 | 29 | 6.1 | 8140 |
| 2005 | 12 | 12 | 210140.63 | 43.21 | 139.33 | 26 | 5.7 | 7657 |
| 2005 | 12 | 21 | 70905.17 | -0.07 | 124.67 | 25 | 6.3 | 8865 |
| 2006 | 1 | 1 | 84713.35 | 4.74 | 95.14 | 51 | 5.7 | 5926 |
| 2006 | 1 | 2 | 10124.39 | 12.36 | 144.31 | 35 | 5.7 | 9885 |
| 2006 | 1 | 3 | 122757.67 | 13.84 | 145.29 | 78 | 5.9 | 9878 |
| 2006 | 1 | 3 | 105304.8 | 51.45 | -168.12 | 10 | 5.5 | 9901 |
| 2006 | 1 | 7 | 22343.59 | 52.42 | 173.61 | 30 | 5.7 | 9088 |
| 2006 | 1 | 15 | 115829.12 | -7.83 | 122.6 | 264 | 6 | 9175 |
| 2006 | 1 | 31 | 191551.59 | 2.7 | 96.07 | 20 | 5.7 | 6149 |
| 2006 | 4 | 15 | 224054.23 | 22.8 | 121.36 | 18 | 5.5 | 7216 |
| 2006 | 5 | 24 | 101107.77 | -2.25 | 139.15 | 30 | 5.7 | 10328 |
| 2006 | 5 | 26 | 225358.92 | -7.96 | 110.45 | 12 | 6 | 8126 |
| 2006 | 7 | 18 | 32752.57 | -0.18 | 124.94 | 37 | 5.8 | 8897 |
| 2006 | 7 | 19 | 15855.18 | -9.22 | 108.37 | 10 | 5.5 | 8040 |
| 2006 | 7 | 23 | 82204.16 | -0.34 | 123.29 | 28 | 5.8 | 8756 |
| 2006 | 7 | 25 | 123923.83 | -9.26 | 108.41 | 10 | 5.6 | 8046 |
| 2006 | 7 | 28 | 74011.84 | 24.18 | 122.53 | 33 | 5.7 | 7248 |
| 2006 | 8 | 6 | 181639.72 | 26.12 | 144.01 | 20 | 6 | 8999 |
| 2006 | 8 | 11 | 205414.37 | 2.4 | 96.35 | 22 | 5.8 | 6194 |
| 2006 | 8 | 12 | 183917.24 | 28.79 | 130.02 | 22 | 5.6 | 7664 |
| 2006 | 8 | 15 | 30511 | -4.67 | 126.73 | 16 | 6.1 | 9344 |
| 2006 | 8 | 20 | 30102.41 | 49.82 | 156.41 | 26 | 5.8 | 8385 |
| 2006 | 8 | 24 | 215036.65 | 51.15 | 157.52 | 43 | 5.9 | 8361 |
| 2006 | 8 | 27 | 171117.47 | 24.95 | 122.94 | 146 | 5.5 | 7244 |
| 2006 | 8 | 31 | 80827.42 | -0.27 | 125.06 | 36 | 6.1 | 8913 |
| 2006 | 9 | 1 | 102517.13 | 53.26 | 159.7 | 51 | 5.7 | 8337 |
| 2006 | 9 | 1 | 120422.17 | 53.97 | -166.39 | 75 | 5.8 | 9708 |
| 2006 | 9 | 5 | 45302.1 | 7.68 | 126.43 | 135 | 5.5 | 8547 |
| 2006 | 9 | 6 | 50027.97 | 61.63 | 168.64 | 7 | 5.5 | 8146 |

| 2006 | 9 | 9 | 41312.03 | -7.21 | 120.11 | 571 | 6 | 8914 |
|------|----|----|-----------|--------|--------|-----|-----|------|
| 2006 | 9 | 16 | 94523.91 | -3.08 | 129.44 | 17 | 5.9 | 9490 |
| 2006 | 9 | 17 | 73011.1 | -17.69 | 41.83 | 10 | 5.5 | 5780 |
| 2006 | 9 | 21 | 185450.05 | -9.05 | 110.36 | 25 | 5.7 | 8195 |
| 2006 | 9 | 24 | 225621.07 | -17.74 | 41.81 | 6 | 5.6 | 5785 |
| 2006 | 9 | 25 | 24337.2 | -0.18 | 124.83 | 35 | 5.5 | 8887 |
| 2006 | 9 | 28 | 13648.33 | 46.46 | 153.36 | 11 | 5.8 | 8418 |
| 2006 | 10 | 23 | 211719.98 | 29.35 | 140.27 | 11 | 6 | 8496 |
| 2006 | 11 | 14 | 142101.32 | -6.39 | 128 | 345 | 5.7 | 9568 |
| 2006 | 11 | 15 | 35227.73 | 4.9 | 127.41 | 80 | 5.5 | 8796 |
| 2006 | 11 | 16 | 62020.77 | 46.36 | 154.47 | 9 | 6 | 8494 |
| 2006 | 11 | 17 | 180312.26 | 28.59 | 129.9 | 22 | 5.9 | 7664 |
| 2006 | 11 | 22 | 111509.62 | 44.15 | 146.78 | 79 | 5.6 | 8127 |
| 2007 | 4 | 20 | 22334.04 | 25.62 | 125.04 | 11 | 5.9 | 7396 |
| 2007 | 4 | 20 | 14556.11 | 25.71 | 125.11 | 9 | 6.3 | 7398 |
| 2007 | 4 | 20 | 193758.23 | 27.47 | 128.38 | 42 | 5.9 | 7592 |
| 2007 | 4 | 21 | 3224.85 | 21.14 | 122.13 | 10 | 5.5 | 7374 |

Teleseismic P receiver functions were computed for most of the 150 teleseismic events as explained in part 3 for each station. A distance (moveout correction) correction was applied prior to stacking to achieve high signal to noise ratio. The P receiver functions were sorted according to their increasing back azimuth. figure 5. shows the whole set of Q components in the 30 s time interval starting from the P-wave onset for VIS and GHG, respectively (from left to the right). The similarity of the waveforms from different events is clear especially at VIS.

The difference in the records at a station are probably mainly due to azimuthal variations. The stacked waveforms (shown at the top) at VIS and GHG are different, implying that the receiver structures at these stations are different. At VIS, there are signals from an upper crust discontinuity at about 2.5 s and from the Moho at about 6.0 s. At GHG, the two clear pulses are the conversions at the base of sediments and the Moho discontinuity about 1.2 s and 5.5 s respectively. figure 6. shows the whole set of the stacked Q-components for all 6 stations.
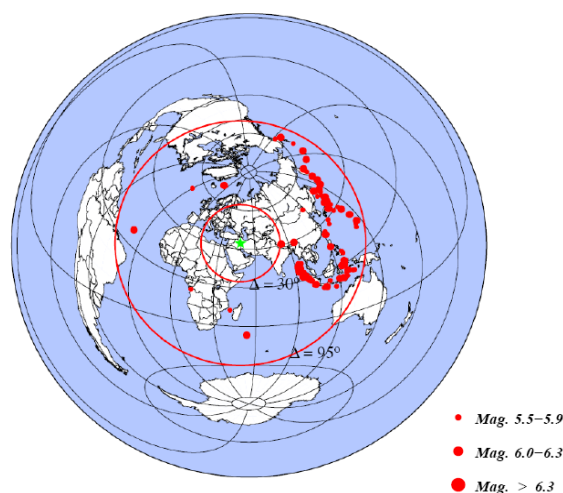


**Figure 4.** Epicenter distribution of earthquakes used to determine P receiver function in this study. The events have magnitude $m_b \geq 5.5$ with epicentral distances between 30-95°.
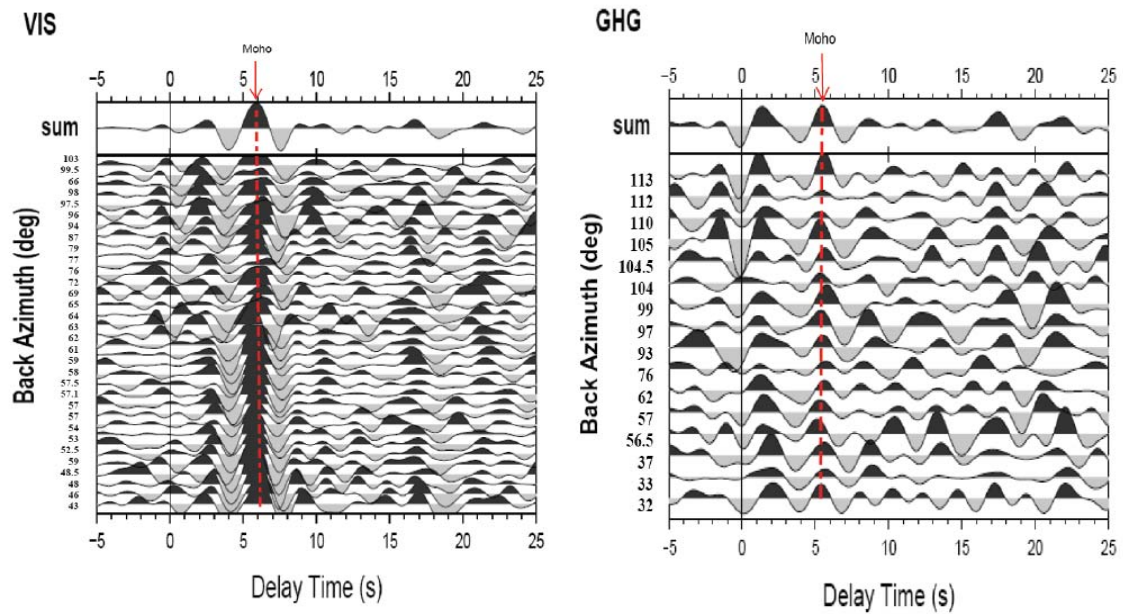
**Figure 5.** An example of the stacking of the P receiver function for station VIS (left) and GHG (right). The trace labeled sum is the stacked receiver function obtained from stacking of individual Q components. Red dashed lines show Ps converted from Moho.
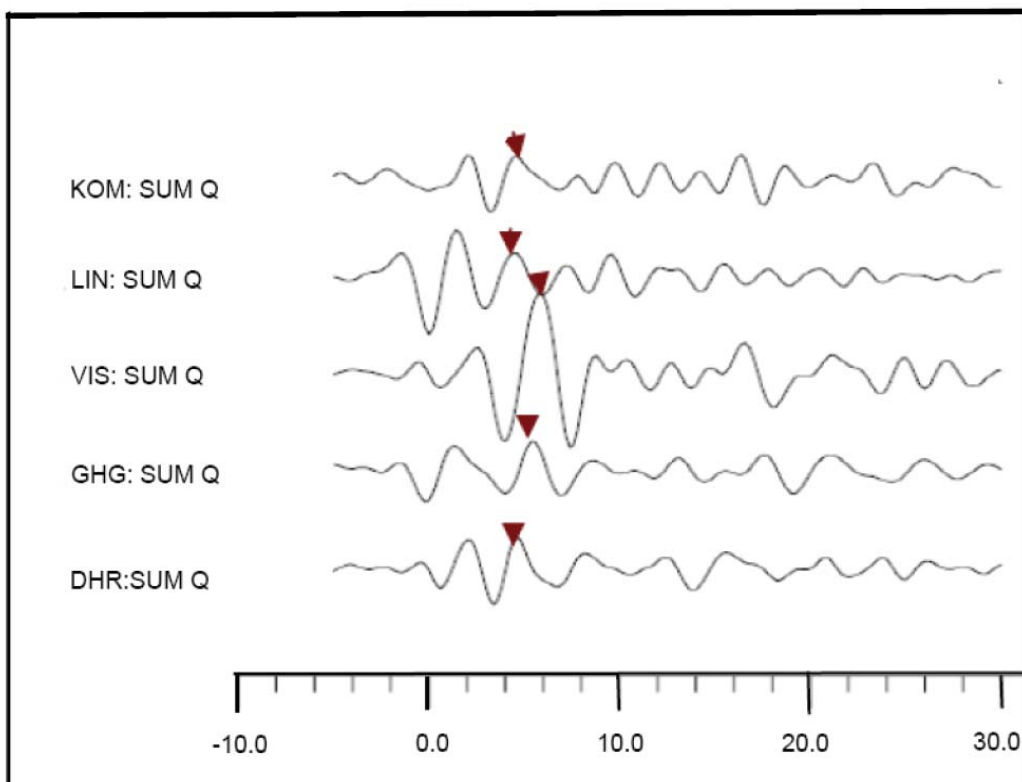


**Figure 6.** The result of stacking P receiver functions for Kermanshah stations. Brown reverse triangles show Ps conversion from Moho.

## 5 DISCUSSION

The applied inversion method is not unique, since it tries to find, by definition models close to the starting model. The inversions were made within a time window from -5 to 30s, which includes all the crustal conversions and strongest multiples. We did the inversion by choosing a different starting model and then adding a priori information. The starting model used for all stations, resulted from the Zhu and Kanamori method in this region (Afsari et al., 2008) and other studies in the Zagros (Paul et al., 2006; Hatzfeld et al, 2003). We carried out the inversion method in two steps. Firstly, we considered 60 km thickness for the crust with

different layer thicknesses (at least each one 2 km thick) with a range of P wave velocity between 5 to 7 kms$^{-1}$ for starting models. We selected models which had good coverage with each other by root mean square less than 0.25s. figure 7 shows two examples of the first step inversion for GHG and VIS stations with two different models. Starting and final models are shown by thin and heavy lines in the left half of each panel, respectively. The dotted line in the right panel is the observed receiver function, the thin line is the theoretical receiver function belonging to the starting model and the heavy line belongs to the final model in the first step.
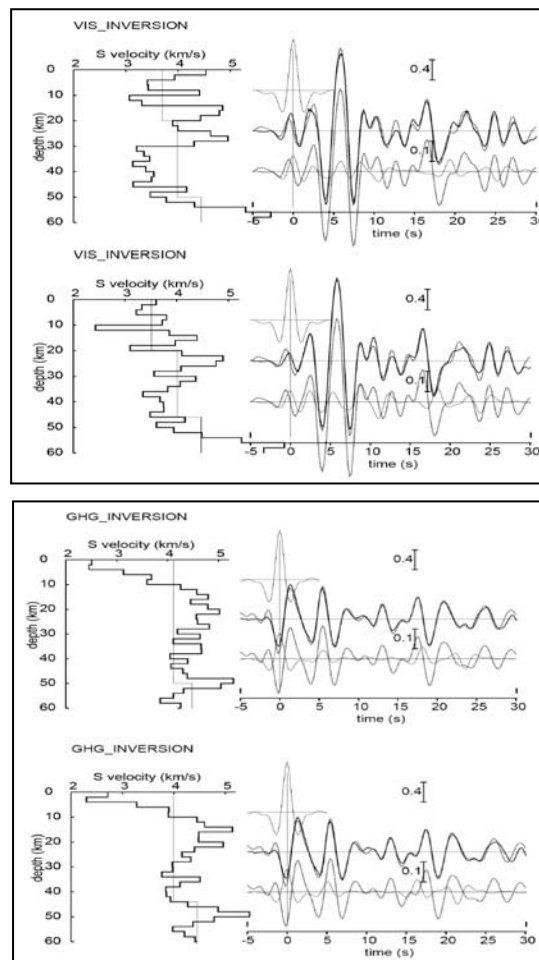


**Figure 7.** Two examples of P receiver functions inversion for VIS station (top) and GHG station (bottom) in the first step with two different initial models. The dotted line in the right panel is the observed receiver function, the thin line is the theoretical receiver function belonging to the starting model and the heavy line belongs to the final model. Root mean square errors from top to bottom are 0.018, 0.015, 0.013 and 0.012 respectively.

In the second step, to obtain optimum model, we considered the average initial models of the first step whose final models had good convergence by the starting model for the second step. In this step, we considered a 2 layered model (according to main converted phases on RFs) for 60 km thickness then examined many different models. Finally, we selected final models which had good coverage with each other by root mean square less than 0.05s. We computed the final velocity model by averaging these models. The final model are two layers, the thickness of the first layer varies from 9 to 18 km, and its S velocity from 3.08 to 3.58 kms$^{-1}$. The thickness and velocity of the second layer are from 24 to 34 km and from 3.80 to 4.21 kms$^{-1}$, respectively. Two examples of receiver functions inversion with two different initial models, input and output models in the first step and final model in the second step are shown in figures 8 to 11 for DHR, VIS, KOM and GHG stations of Kermanshah Telemetry Network. Blue lines represent input and output models in each step. Dark blue lines show the average model in each step. The violet arrow shows the

Moho depth in the final model. Table 3 shows final results P receiver functions inversion for the Kermanshah region.

## 6 CONCLUSIONS

The receiver function method has proved to be very useful for the determination of crustal discontinuities. We obtained new informations from the determined P receiver functions at five short period stations of Kermanshah Network. The inversion method resulted in shear wave velocity structure within the crust. Our modeling showed that the thickness of the crust beneath the northwest of the Zagros is approximately 42 km. Even though we found a thick crust of 52 km beneath the station VIS located in the central part of the study area. Due to the convergence of the Arabian plate and Eurasiaw plate, the crustal thickening is taking place in the region (Aghanabati, 1383). Thus, the results of our study are in agreement with the geological evidence. Also these results are consistent with the results of previous studies (Hatzfeld et al., 2003; Paul et al., 2006; Afsari et al., 2008).

**Table 3.** final results of P receiver function inversion in Kermanshah region.

| Veis | Ghaleghazi | Lien | Komasi | Dehrash | Station name | |
|---|---|---|---|---|---|---|
| VIS | GHG | LIN | KOM | DHR | Station code | |
| 18 | 9 | 13 | 14 | 16 | 1 | thickness (km) |
| 34 | 35 | 26 | 26 | 24 | 2 | |
| 0.24±3.18 | 0.23±3.08 | 0.28±3.02 | 0.20±3.49 | 0.24±3.37 | 1 | S velocity (kms$^{-1}$) |
| 0.03±4.21 | 0.29±3.84 | 0.26±3.80 | 0.27±3.90 | 0.03±3.96 | 2 | |
| 0.38±5.80 | 0.33±4.64 | 0.40±4.34 | 0.36±4.70 | 0.15±4.64 | S Velocity under Moho) ((kms$^{-1}$) | |
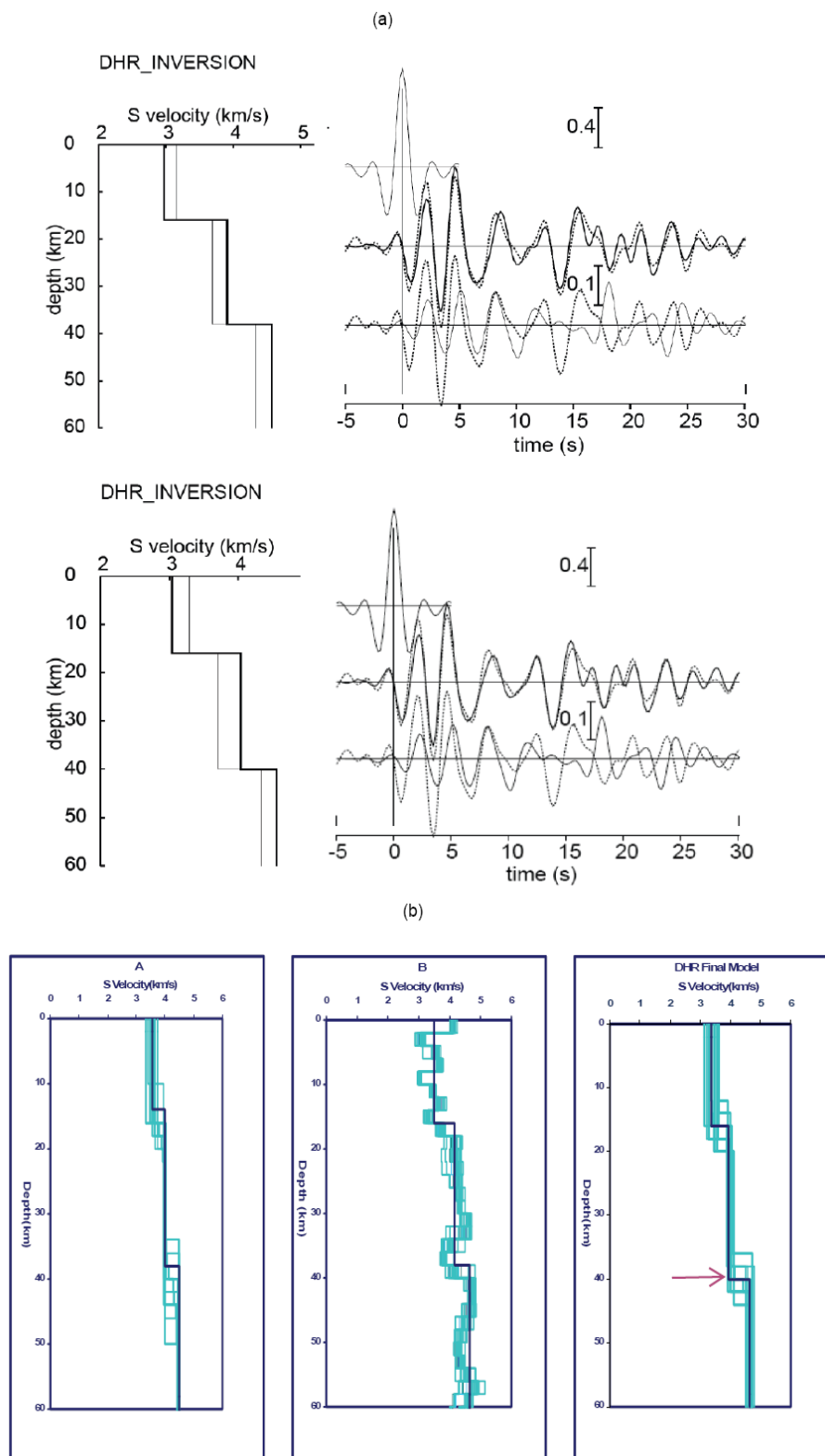
**Figure 8.** Two examples of receiver functions inversion for DHR station in the second step with two different models. Root mean square errors are 0.030 and 0.029 respectively. b) From left to right input and output model in the first step and the final model in the second step are shown. Dark blue lines and the violet arrow represent average models and Moho depth in the final model respectively.
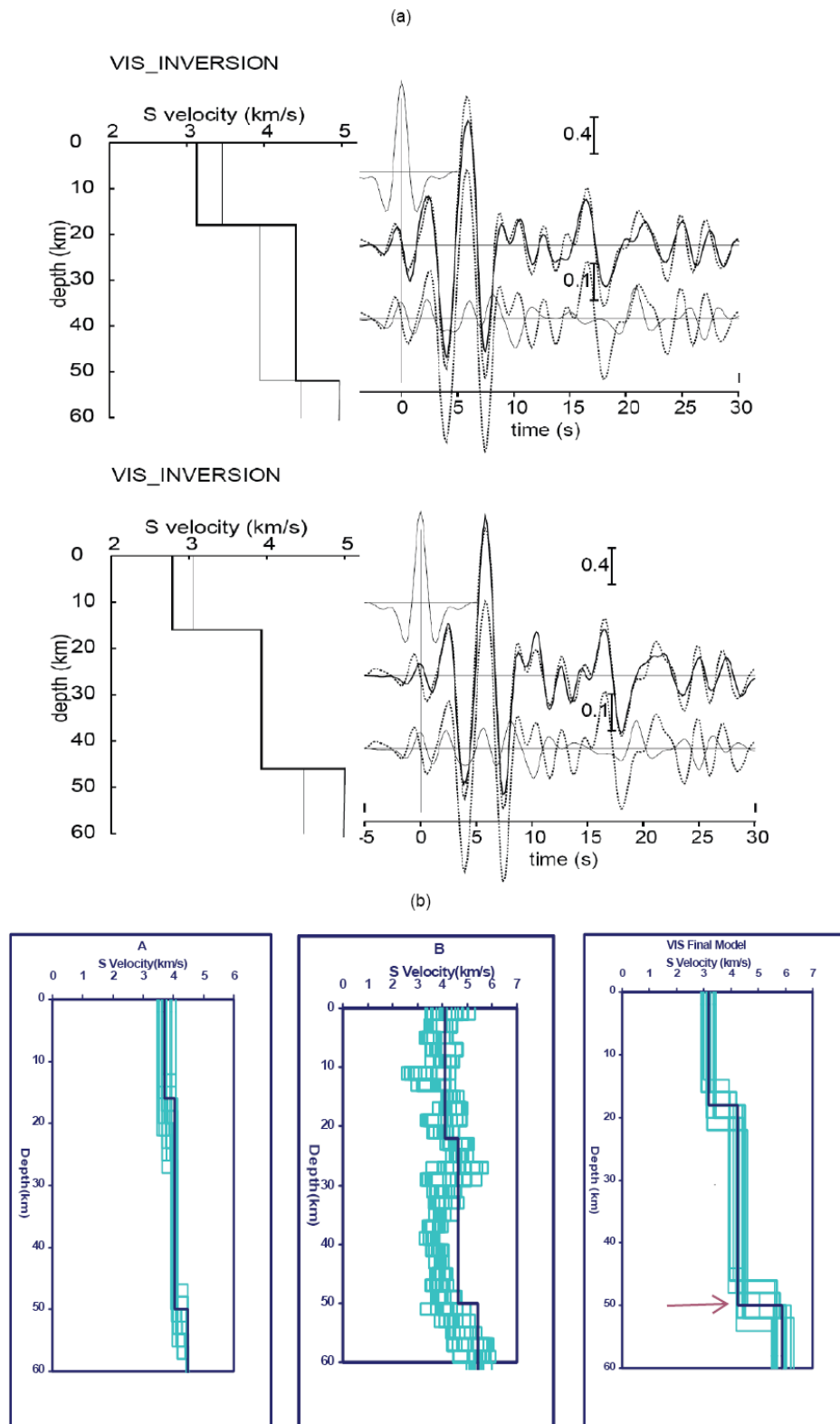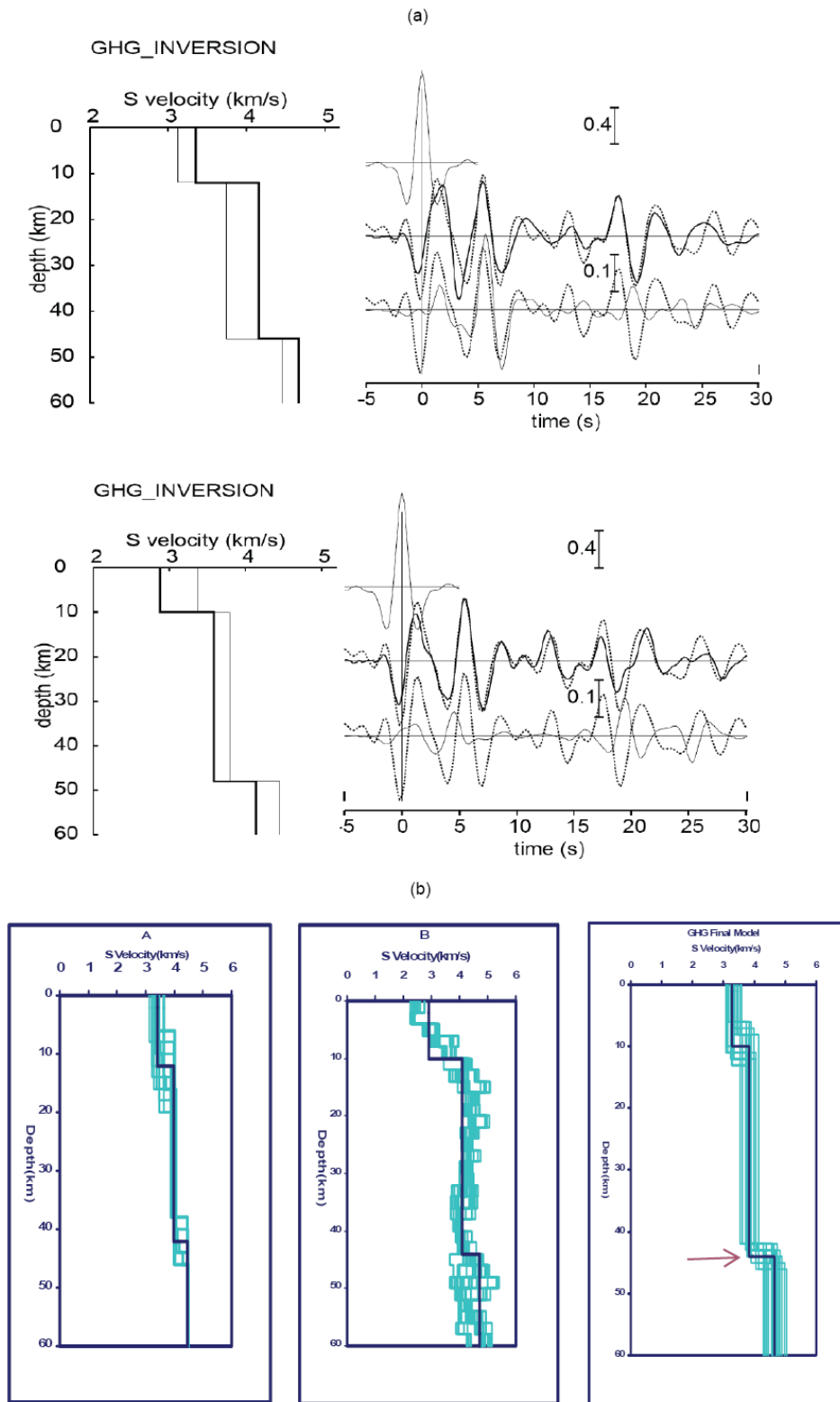
**Figure 9.** Two examples of receiver functions inversion for VIS station in the second step with two different models. Root mean square errors are 0.034 and 0.033 respectively. b) From left to right input and output model in the first model in the second step are shown. Dark blue lines and the violet arrow represent average models and Moho depth in the final model respectively.
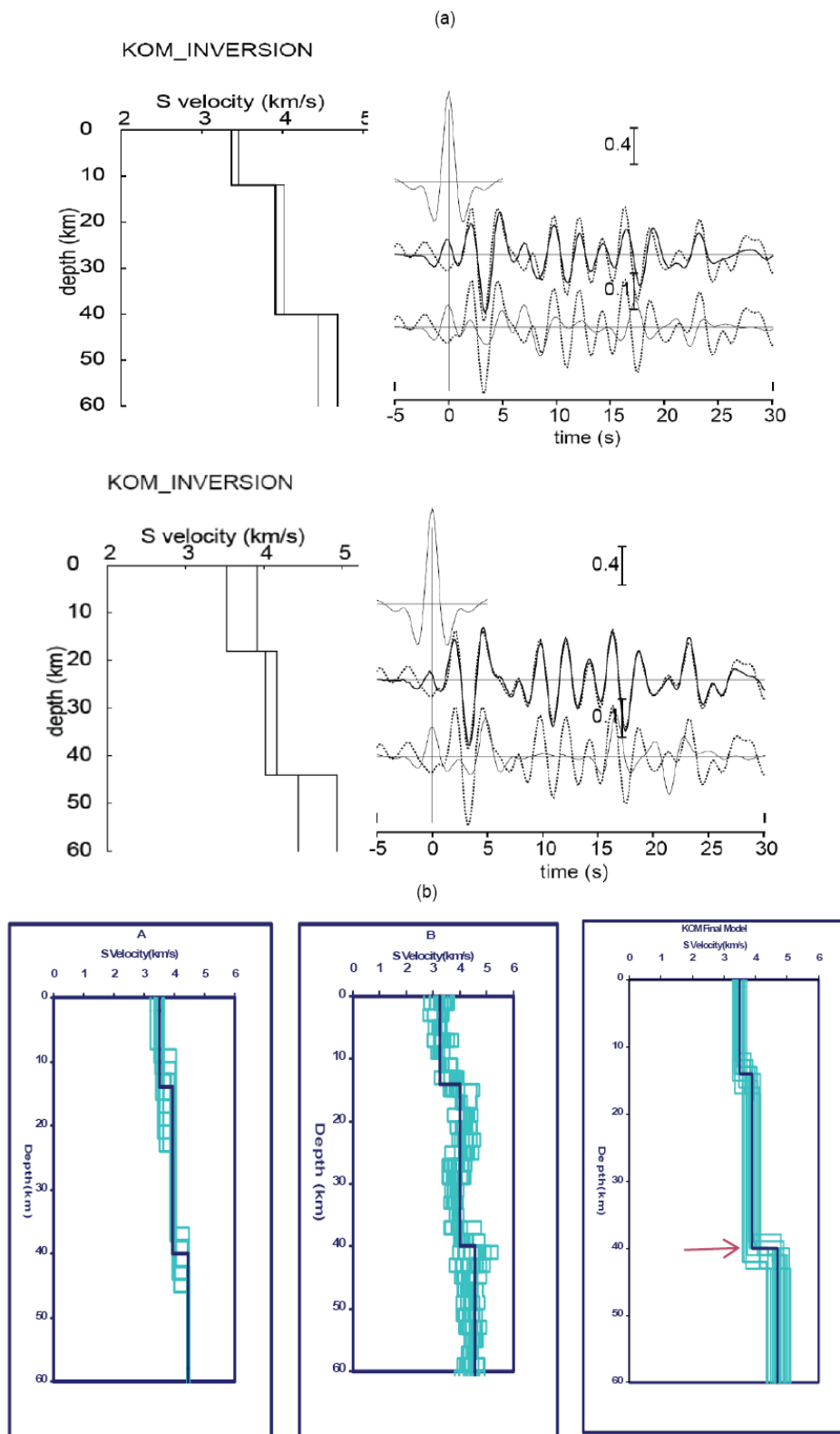
**Figure 10.** Two examples of receiver functions inversion for KOM station in the second step with two different models. Root mean square errors are 0.040 and 0.032 respectively. b) From left to right input and output model in the first model in the second step are shown. Dark blue lines and the violet arrow represent average models and Moho depth in the final model respectively.

**Figure 11.** (a) Two examples of receiver functions inversion for GHG station in the second step with two different models. Root mean square errors are 0.035 and 0.030 respectively. (b) From left to right input and output model in the first model in second step are shown. Dark blue lines and the violet arrow represent average models and Moho depth in the final model respectively.

## 7. ACKNOWLEDGMENTS

## REFERENCES

Aghanabati, A, 1383, Geology of Iran, Publ. Geological Survey of Iran, 586 pp.

Ammon, C. J., 1990, On the nonuniqueness of receiver function inversion, J. Geophys. Res, **95**, 2504-2510.

Afsari, N., Sodoudi, F., Gheitanchi, M. R., and Kaviani, A, 2008, Moho depth variations and Vp/Vs ratio in Northwest of Zagros (Kermanshah region) using teleseismic receiver functions, J. Geosci. (GSI), In press.

Berberian, M., 1995, Master blind thrust faults hidden under the Zagros folds: active basement tectonics and surface morphotectonics, Tectonophysics, **241**, 193-224.

Berberian, M., and Tcahlenko, J., 1976a, Earthquakes of the southern Zagros (Iran): Bushehr region, Geol. Surv. Iran. **39**: 343-370.

Berberian, M. and Tcahlenko, J., 1976b, Earthquakes of Bandar Abbas- Hajiabad region (Zagros, Iran), Geol. Surv. Iran, **39**: 371-396.

Birch, F., 1961, The velocity of comressional waves in rocks to 10 kilobars, Part 2. J Geophys. Res., **66**, 2199-2224.

Burdick, L. J. and. Langston, C. A, 1977, Modeling crust-structure though the use of converted phases in teleseismic body-waveforms, B. Seimol. Soc. Am, **67**, 677-691.

Dehgani, G. and Makris, J., 1984, The gravity field and crustal structure of Iran, N. Jb. Geol. Palaont Abh., **168**: 215-229.

Haskell, N. A., 1962, Crustal reflections of plane P and SV waves, J. Geophys. Res., **67**, 4751-4767.

Hatzfeld, D., Tatar, M., Priestley, K., and Ghafory-Ashtiany, M, 2003, Seismological constrains on the crustal structure beneath the Zagros mountain belt (Iran), Geophys. J. Int. **155**, 403-410.

Jackson, J. A., 1980, Reactivation of basement faults and crustal shortening in orogenic, Nature, **283**, 343-346.

Jackson, J. A., 1992, Partitioning of strike-slip and convergent motion between Eurasia and Arabia in Eastern Turkey and the Caucasus, J. Geophys. Res. **97** (B9): 12471-12479.

Jackson, J. A. and McKenzie, D. P., 1984, Active tectonic of the Alpine- Himalayan belt between Western Turkey, Geophys. J. Roy Astron. Soc., **57**: 209-229.

Kaviani, A., Paul, A., Bourova, E., Hatzfeld, D., Pedersen, H., and Mokhtari, M., 2007, A strong seismic velocity contrast in the shallow mantle across the Zagros collision zone (Iran), Geophys. J. Int., **171**, 399-410. doi: 10.1111/j.1365-246X. 2007.03535. x.

Kennett, B. L. N., and Engdahi, E. R., 1991, Travel times for global earthquake location and phase identification, Geophys. J. Int. **105**, 429-465.

Kind, R., Kosarve, G., and Peterson, N. V., 1995, Receiver function at the stations of the German Regional Seismic Network (GRSN), Geophys. J. Int., **121**,191-202.

Langston, C.A., 1977, The effect of planner dipping structure for constant ray parameter, BSSA, **67**,1029-1050.

Langston, C. A., 1979, Structure under Mount Rainier, Washington, inferred from teleseismic body waves, J. Geophys. Res., **84**, 4749 – 4762.

Owens, T. J., Zandt, G. and Taylor, S. R., 1984, Seismic evidence for an ancient rift beneath the Cumberland Plateau, Tennessee: A detailed analysis of broadband teleseismic P waveforms, J. Geophys. Res, **89**, 7783-7795.

Owens, T. J., Taylor, S. R. and Zandt, G., 1987, Crustal structure at regional seismic test network stations determined from inversion of broadband teleseismic P waveforms, B. Seismol. Soc. Am. **77**, 631-662.

Paul, A., Kaviani, A., Hatzfeld, D., Vergne, J., and Mokhtari, M., 2006, Seismological

evidence for crustal–scale thrusting in Zagros mountain belt (Iran). Geophys, J. doi; 10.1111/j.1365-246X.2006.02920.x.

Phinney, R. A., 1964, Structure of the Earth's crust from spectral behavior of long-period body waves, J. Geophys. Res. **69**, 2997-3107.

Snyder, J., D. B., and Barazangi, M., 1986, Deep crustal structure and flexture of the Arabian plate beneath the Zagros collisional mountain belt as inferred from gravity observations, Tectonics, **5**, 361-373.

Tchalenko, J. S., and Braud., J., 1974, Seismicity and structure of the Zagros (Iran):The Main Recent Fault between 33º and 35º N, Philos. T. Roy. Soc. Lond., A **227**, 1-25.

Vernant, P., Niloforoushan, F., Hatzfeld, D., Abbassi, M. R., Vigny, C., Masson, F., Nankali, H., Martinod, J., Ashtiani, A., Bayer, R., Tavakoli, F., and Chery, J., 2004, Present- day crustal deformation and plate kinematics in the Middle East constrained by GPS measurements in Iran and northern Oman, Geophys. J. Int. **157**, 381-398.

Vinnik, L. P., and Kosarev, G. L., 1981, Determination of crustal parameters from observations of teleseismic body waves, Proc. Acad. Sci. USSR, **261**, 1091-1095.

Zhu, L., and Kanamori, H., 2000, Moho depth variation in southern California from telesiesmic receiver, J. Geophys. Res, **105**, 2969-2980.